THE JOURNAL OF PHYSICAL CHEMISTRY C

Article

Cite This: J. Phys. Chem. C XXXX, XXX, XXX−XXX

pubs.acs.org/JPCC

Vacancy-Driven Stabilization of the Cubic Perovskite Polymorph of $CsPbI_3$

Yun-Hyok Kye,[†] Chol-Jun Yu,*[,†] Un-Gi Jong,[†] Kum-Chol Ri,[†] Jin-Song Kim,[†] Song-Hyok Choe,[†] Song-Nam Hong,[†] Shuzhou Li,[‡] Jacob N. Wilson,[§] and Aron Walsh*[,§]

[†]Chair of Computational Materials Design, Faculty of Materials Science, Kim Il Sung University, Ryongnam-Dong, Taesong District, Pyongyang, Democratic People's Republic of Korea

[‡]School of Materials Science and Engineering, Nanyang Technological University, Nanyang Avenue, 639798, Singapore

[§]Department of Materials, Imperial College London, London SW7 2AZ, United Kingdom

Supporting Information

ABSTRACT: The inorganic halide perovskite $CsPbI_3$ has shown great promise for efficient solar cells, but the instability of its cubic phase remains a major challenge. We present a route for stabilizing the cubic α-phase of $CsPbI_3$ through the control of vacancy defects. Analysis of the ionic chemical potentials is performed within an ab initio thermodynamic formalism, including the effect of solution. It is found that cation vacancies lead to weakening of the interaction between Cs and PbI_6 octahedra in $CsPbI_3$, with a decrease in the energy difference between the α- and δ-phases. Under I-rich growth conditions, which can be realized experimentally, we predict that the formation of cation vacancies can be controlled. Other synthetic strategies for cubic-phase stabilization include the growth of nanocrystals, surface capping ligands containing reductive functional groups, and extrinsic doping. Our analysis reveals mechanisms for polymorph stabilization that open a new pathway for structural control of halide perovskites.

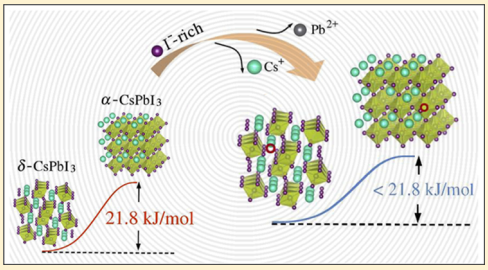

INTRODUCTION

Metal halide perovskite solar cells (PSCs) are widely recognized as a propitious alternative photovoltaic (PV) technology, with noticeable improvements in power conversion efficiency (PCE) and device stability over the past decade.[1] The most promising PSCs, the so-called hybrid halide perovskites, feature organic monovalent cations—commonly methylammonium ($CH_3NH_3^+$; MA), formamidinium ($CH_3(NH_2)_2^+$; FA), or a combination of the two—located at the center of corner-sharing metal halide octahedra. The route to commercialize these materials is currently hindered by device instability resulting from unavoidable hygroscopicity and thermodynamic effects.

Partial substitution of Cs^+ for MA^+ or FA^+ has been reported to reduce the effect of hygroscopicity and, moreover, the tendency for the visible light absorbing α-$FAPbI_3$ perovskite phase to decompose into the wider band gap δ-$FAPbI_3$ nonperovskite phase.[2−4] Density functional theory (DFT) calculations contemplating the effect of doping α-$FAPbI_3$ with MA^+, Cs^+, or Rb^+ suggest that substituting 50% of the FA^+ cations for Cs^+ could rationalize the improved phase stability.[5,6] Experimentally, however, modifying $FAPbI_3$ with more than 20−30% Cs^+ results in chemical segregation into distinct $CsPbI_3$ and $FAPbI_3$ regions and subsequent transition of both materials from the black perovskite α-phase to the yellow nonperovskite δ-phase.[2,3,7,8] The lower solubility limit observed experimentally may be rationalized by considering the characteristic mismatch in the lattice parameters of Cs and FA, which leads to local strain variations difficult to be accounted for theoretically in atomistic simulations.[7,8] The development of alternative thermochemical routes to improve the solubility of Cs in hybrid PSCs may be a route to further enhance the performance of these devices.

In recent years, inorganic cesium lead halide perovskites ($CsPbX_3$; X = Cl, Br, and I) have emerged as promising constituents for optoelectronic devices with improved stability performance. The application of $CsPbX_3$ in devices such as single-, multi-junction, and tandem solar cells;[9−11] photodetectors;[12,13] and light-emitting diodes[14,15] has been reported. The most appealing cesium lead halide material for solar cell application is α-$CsPbI_3$, which, because of its appropriate band gap (ca. 1.7 eV) and other promising optoelectronic properties,[10,16] has realized a PCE of 11.7%. However, the phase transition from α-$CsPbI_3$ into the nonperovskite δ-$CsPbI_3$ spontaneously occurs at room temperature, as mentioned above, because of the lower internal energy (by 17 kJ/mol).[17,18] The δ-phase of $CsPbI_3$ is inappropriate for solar application as it has a band gap of 2.8 eV at room temperature.[16] Experimental observations clarify the true nature of cubic $CsPbI_3$ as a dynamical average state between

Received: February 18, 2019
Revised: March 18, 2019
Published: March 22, 2019

DOI: 10.1021/acs.jpcc.9b01552
J. Phys. Chem. C XXXX, XXX, XXX−XXX

the symmetry-broken local minima phases.[19] That is, α-$CsPbI_3$ is a metastable phase located on the saddle point of a double-well potential whose minima are located by equivalent δ-phases[20] or tilted cubic phases.[21] Thus, the stability of the apparent α-phase is determined by the potential energy barrier for the lattice distortion. As such, the effect of anharmonicity on the lattice dynamics of cubic $CsPbI_3$ has also been emphasized.[20−22]

Many approaches to improve the synthesis and room-temperature stability of α-$CsPbI_3$ crystalline thin films, mainly through reducing crystal size, have been proposed.[10,23] These include (1) Br^- or Cl^- incorporation into $CsPbI_3$,[24,25] (2) addition of hydroiodic acid (HI) into precursor solutions,[10,16,26] (3) decreasing the crystal size (nanocrystal quantum dots)[11,17] and dimension (quasi two-dimensional (2D) or one-dimensional),[10,26,27] and (4) anion exchange from colloidal and sintered $CsPbBr(Cl)_3$ nanocrystals (NCs).[18,28,29] Replacing conventional surface capping ligands (SCLs), such as oleic acid (OA), with other solvating agents has also been shown to produce α-phase $CsPbI_3$ with high NC quality and improved stability. Specifically, the agents trioctyl phosphine (TOP),[30,31] bis(2,2,4-trimethylpentyl)phosphinic acid (TMPPA),[32] diphenyl phosphinic acid (DPPA),[33] iminodibenzoic acid (IDA),[15] and poly-vinylpyrrolidone (PVP) have been shown to produce stable cubic grains with size up to micrometer scale.[34] Replacing lead ions with divalent (Ca^{2+})[23] or trivalent (Bi^{3+}, Sb^{3+}) cations[35,36] has also been reported as an alternative route to enhance the α-phase stability at a relatively low temperature (~100 °C).

Although the justification of each individual strategy is reasonable, they are often elusive or incompatible with other models. For example, α-$CsPbI_3$ NCs were believed to be stable on account of either (1) Cs replacement by large organic amine cations which increase the tolerance factor or (2) sufficient surface energy gain compensating the internal energy difference.[9,17] Neither regime has been supported by a quantitative thermodynamic demonstration, however. Moreover, fabrication techniques employing iodine exchange and surface passivation, which produce stable crystalline samples of α-$CsPbI_3$ with average grain size over 1 μm,[18,34] cast a doubt on whether the α-phase stability is only related to the crystal size and surface energy. Very recently, Marronnier et al. found metastable β- and γ-perovskite phases, with space groups $P4/mbm$ and $Pbnm$, respectively, when heating above the melting point (757 K) and supercooling to room temperature.[21] The authors explain that the nanosize effect results from the prevention of polar disorder of the δ-phase.[21] This view contradicts the high temperature instability of δ-phase, as the entropic gain from polar disorder is expected to improve its stability at high temperature.

The addition of HI has been qualitatively explained to accelerate the crystallization of smaller grains owing to the reduced solubility of Cs precursors and to the increased crystal strain.[9,16] An alternative report suggests instead that the effect is related to a reduction of the transition energy barrier for α-phase.[10] The inclusion of surfactants has been experimentally observed to manifest large increases in PCEs, from 2.9[16] to 11.8%,[10] which provides a hint toward the relationship between defects and the stability of $CsPbI_3$. While it is stabilizing in terms of Gibbs free energy or an increased activation energy for phase transformation, compensation of the internal energy difference is the key factor for rationalizing the α-phase stability. However, because the fabrication of $CsPbI_3$ is commonly based on solution processing, the stabilization of the α-phase should be studied and explained in correlation with the thermochemistry of solvents, anti-solvents, surfactants, and other concomitants such as PbI_2, CsI, and HI.

In this work, we develop and apply an ab initio atomistic thermodynamic formalism for defects in halide perovskites that considers solvated ions in aqueous or electrolytic solutions. By doing so, we are able to reproduce experimental situations and make realistic predictions. Chemical potentials of solvated ions (Cs^+, Pb^{2+}, and I^-) as a function of temperature and concentration are determined quantitatively and referenced to the DFT total energies and experimental Gibbs free energies of formations. Using this formalism, we study the defect physics of vacancies in α- and δ-$CsPbI_3$ in equilibrium in a solution environment. It is predicted that the stability of α-$CsPbI_3$ can be enhanced through the formation of charged cation vacancies. We suggest that cation vacancies are likely to be formed by introducing I^--rich conditions, surface treatments that contain more reductive or less Lewis acidic functional groups, and n-type doping.

METHODS

Ab Initio Thermodynamics of Defects Including Solvent Effects. The study of point defects, such as vacancies, interstitials, and antisites, is often performed using ab initio thermodynamics. The formation energy (ΔG) of a point defect D in charge state q is given as a function of both the atomic chemical potential, μ, and the Fermi energy, E_F. The atomic chemical potential is referenced to that of an element in its standard state, for example, Pb(s) or I(s). The Fermi energy is given with respect to the valence band maximum (VBM) of the perfect crystal and represents the electron reservoir. For moderate defect concentrations (<1%) and temperatures (<1000 K), the vibrational entropic effects in crystalline solid are often negligible.[37] Consequently, the defect formation energy is usually considered equivalent to the formation enthalpy, ΔH_f, which can be written as[38]

$$\Delta G[D^q] \approx \Delta H_f[D^q] = E[D^q] - E_{perf} - \sum_i n_i\mu_i + qE_F + E_{corr} \quad (1)$$

Here, E_{perf} and $E[D^q]$ are the total energies of a perfect and a defect-containing supercell and n_i is the number of added or removed i-type species. E_{corr} is a correction energy that considers the finite size effect of periodic supercells, the effect of band-filling, and electrostatic potential alignment. In this scheme, thermodynamic constraints on defect formation are indirectly reflected on the chemical potentials of constituent elements in certain environmental conditions during synthesis or post-processing.

Previous studies contemplating the effect of growth conditions on defect formation in halide perovskites have considered the DFT total energies of precursors, such as CsI and PbI_2.[39−43] However, the ionic nature of chemical bonding in the metal halide octahedra[44] and the electrolyte solution environment of synthesis or of dissociation cannot be completely described through this procedure.[9,16,17] Consequently, only qualitative justification for the reduction of recombination centers, for example, by means of iodine-rich or -poor growth conditions, has been suggested.[40]

DOI: 10.1021/acs.jpcc.9b01552
J. Phys. Chem. C XXXX, XXX, XXX−XXX

To accurately describe the thermodynamics of fabrication, the chemical potentials should be those of solvated ions rather than neutral atoms in their standard state. Therefore, with the motivation of studying the defect physics of $CsPbI_3$, we modify eq 1 to account for the effect of solution that provides a reservoir of charged ions.[38,45−47] The revised equation takes the form

$$\Delta G_f[D^q](T, P) \approx E[D^q] - E_{perf} - \sum_i n_i \mu_i^{q_i}(T, P) + \left(q - \sum_i n_i q_i\right) E_F + E_{corr} \quad (2)$$

where ΔG is the temperature (T)- and pressure (P)-dependent Gibbs free energy of formation and $\mu_i^{q_i}$ is the chemical potential of the solvated ion, i, that is surrounded by a solution which is in charge state q_i. Because of the lack of data for the thermodynamics of electrolyte solutions, we assume an aqueous solution environment, as in ref 21 when applying eq 2 for a solution environment that is composed of coexisting α- and δ-$CsPbI_3$. The success of eq 2 is therefore dependent on whether $(\mu_i^{q_i})_{aq}$ can be accurately determined by consideration of external parameters alone, such as ion concentration and solution pH.

The Gibbs free energy of formation for the relevant ions in aqueous solution are determined, by definition, from the following reactions:[48,49]

$$(Cs)_s + (H^+)_{aq} \rightleftharpoons (Cs^+)_{aq} + \frac{1}{2}(H_2)_g \quad (3)$$

$$(Pb)_s + 2(H^+)_{aq} \rightleftharpoons (Pb^{2+})_{aq} + (H_2)_g \quad (4)$$

$$\frac{1}{2}(I_2)_s + \frac{1}{2}(H_2)_g \rightleftharpoons (I^-)_{aq} + (H^+)_{aq} \quad (5)$$

where the subscripts refer to the state of the ion, which may be either solid (s), aqueous (aq), or gaseous (g). The temperature-dependent chemical potentials for each of the reactants and products that feature in eqs 3−5 may be related as follows:

$$(\mu_{Cs}{}^{+})^0_{aq} - (\mu_{H}{}^{+})^0_{aq} = (\Delta G_f{}^{Cs^+})^0_{aq} + (\mu_{Cs}{}^{+})^0_s - \frac{1}{2}(\mu_{H_2})^0_g \quad (6)$$

$$(\mu_{Pb}{}^{2+})^0_{aq} - 2(\mu_{H}{}^{+})^0_{aq} = (\Delta G_f{}^{Pb^{2+}})^0_{aq} + (\mu_{Pb})^0_s - (\mu_{H_2})^0_g \quad (7)$$

$$(\mu_{I}{}^{-})^0_{aq} + (\mu_{H}{}^{+})^0_{aq} = (\Delta G_f{}^{I^-})^0_{aq} + \frac{1}{2}(\mu_{I_2})^0_s + \frac{1}{2}(\mu_{H_2})^0_g \quad (8)$$

Here, the superscript, 0, refers to the environmental condition of standard pressure (1 atm). Values for $(\Delta G_f{}^{Cs^+})^0_{aq}$, $(\Delta G_f{}^{Pb^{2+}})^0_{aq}$, and $(\Delta G_f{}^{I^-})^0_{aq}$ may be taken from standard tables, as in the hypothetical ideal solution with a molality of m = 1 mol/kg.[49] The mathematical procedure for evaluating the chemical potentials of ions in the solid and gaseous state from DFT calculations[50] or from experimental measurement[51] is as follows:

$$\mu^0(T) = H^0(T) - TS^0(T) = H^0(0) + H^0(T) - H^0(0) - TS^0(T) \quad (9)$$

$$\approx E_{DFT} + \Delta\mu^0(T) \quad (10)$$

It is then necessary to introduce a final equation to determine the four unknown chemical potentials on the left-hand sides of eqs 6−8. Any additional ionic reaction equation cannot be linearly independent of eqs 6−8. Therefore, we employ an approximate solving method, performed by contemplating the dissociation reactions for PbI_2 and CsI

$$(PbI_2)_s \rightleftharpoons (Pb^{2+})_{aq} + 2(I^-)_{aq} \quad (11)$$

$$(CsI)_s \rightleftharpoons (Cs^+)_{aq} + (I^-)_{aq} \quad (12)$$

The change in Gibbs free energies for these dissociation reactions is given by

$$(\Delta G_{dis}{}^{PbI_2})^0(T) = (\Delta G_f{}^{Pb^{2+}})^0_{aq}(T) + 2(\Delta G_f{}^{I^-})^0_{aq}(T) - (\Delta G_f{}^{PbI_2})^0_s(T) \quad (13)$$

$$(\Delta G_{dis}{}^{CsI})^0(T) = (\Delta G_f{}^{Cs^+})^0_{aq}(T) + (\Delta G_f{}^{I^-})^0_{aq}(T) - (\Delta G_f{}^{CsI})^0_s(T) \quad (14)$$

such that the additional equations may be written as

$$(\mu_{Pb}{}^{2+})^0_{aq}(T) + 2(\mu_{I}{}^{-})^0_{aq}(T) = (\Delta G_{dis}{}^{PbI_2})^0(T) + (\mu_{PbI_2})^0_s(T) \quad (15)$$

$$(\mu_{Cs}{}^{+})^0_{aq}(T) + (\mu_{I}{}^{-})^0_{aq}(T) = (\Delta G_{dis}{}^{CsI})^0(T) + (\mu_{CsI})^0_s(T) \quad (16)$$

Here, values for $(\mu_{PbI_2})^0_s$ and $(\mu_{CsI})^0_s$ may be approximated by application of eqs 9 and 10. Solving the set of simultaneous equations, eqs 6−8, 15, and 16, using a constrained linear least-squares method, returns the chemical potential of the ions with minimal errors.

It is also necessary to account for constraints which are physically imposed on the chemical potentials. First, the formation energy of a vacancy must be positive in order to ensure that spontaneous dissociation does not occur, leading to

$$(\mu_i^{q_i})^0_{aq}(T) \geq E_{perf} - E[D^{-q_i}] - E_{corr} \quad (17)$$

Second, it has been experimentally shown that $CsPbI_3$ can be produced from the three constituent ions at standard molalities.[17,21] This imposes the additional constraint

$$(\mu_{Cs}{}^{+})^0_{aq}(T) + (\mu_{Pb}{}^{2+})^0_{aq}(T) + 3(\mu_{I}{}^{-})^0_{aq}(T) \geq (\mu_{CsPbI_3})^0_s(T) \quad (18)$$

Practically, molar concentrations of solvated ions in an equilibrium state can be measured and related to the chemical potentials as follows:[48,51]

$$(\mu_i^{q_i})_{aq}(T, P) \cong (\mu_i^{q_i})^0_{aq}(T) + k_B T \ln(a_i) = (\mu_i^{q_i})^0_{aq}(T) + k_B T \ln\left(\lambda_i \frac{m_i}{m_i^0}\right) \quad (19)$$

where k_B is the Boltzmann constant. The relative molal activity, a_i, and molal activity coefficient, λ_i, are introduced to account for the nonideality of physical solution and relate the molality m_i to the chemical potential in connection with the standard state (m_i^0 = 1 mol/kg).[49] Pressure is neglected on the

DOI: 10.1021/acs.jpcc.9b01552
J. Phys. Chem. C XXXX, XXX, XXX−XXX

Table 1. Optimized Lattice Constants of Crystals and Bond Lengths of Molecules, and DFT Total Energies and Chemical Potentials (E_{DFT} and $\Delta\mu^0$) of Compounds Per Formula Unit (f.u.) Derived at Standard Conditions (T = 298 K and P = 1 atm)

		lattice constants/bond lengths (Å)			
compound	phase	cal.	exp.	E_{DFT} (eV/f.u.)	$\Delta\mu^0$ (eV/f.u.)
α-$CsPbI_3$	$Pm\bar{3}m$	a = 6.24	a = 6.18[a]	−11.48	−0.11[e]
δ-$CsPbI_3$	$Pnma$	a = 10.42, b = 4.75, c = 17.66	a = 10.43, b = 4.79, c = 17.76[b]	−11.71	−0.20[e]
PbI_2	$P\bar{3}m1$	a = 4.46, c/a = 1.70	a = 4.56, c/a = 1.53[c]	−7.17	−0.34[d]
CsI	$Pm3m$	a = 4.51	a = 4.57[d]	−4.35	−0.18[d]
Pb	$Fm\bar{3}m$	a = 4.93	a = 4.95[d]	−3.45	−0.13[d]
Cs	$Im\bar{3}m$	a = 5.99	a = 6.14[d]	−0.31	−0.18[d]
I_2	$Cmca$	a = 7.51, b = 4.38, c = 9.63	a = 7.18, b = 4.71, c = 9.81[d]	−1.91	−0.22[d]
I_2	gas	d_{I-I} = 2.656	d_{I-I} = 2.666[d]	−1.26	−0.70[d]
H_2	gas	d_{H-H} = 0.759	d_{H-H} = 0.741[d]	−6.37	−0.32[d]

[a]Reference 16. [b]Reference 57. [c]Reference 51. [d]Reference 49. [e]Reference 58.

assumption of incompressibility of the solution system. Most reported syntheses of $CsPbI_3$ are performed using a non-aqueous solvent, such as DMSO or DMF. However, these solvents have comparable solubility parameters to those of water,[52] making the assumption of aqueous media acceptable.

For the stability comparison between the α- and δ-phases with respect to the defect formation, we adopt the following definition:

$$E_{st}[D^q] \equiv \Delta G[D^q](T, P) - \Delta G_{perf}(T, P) \approx \Delta E[D^q] - \Delta E_{perf} \quad (20)$$

that represents the relative stability improvement (<0) or decrease (>0) of α-phase over δ-phase $CsPbI_3$ induced by defect formation.

Defect Calculation Setup. We employ a supercell approach to simulate the effect of defect formation in extended crystals. Total energy calculations were performed within the framework of DFT using the projector augmented wave method[53] and PBEsol functional[54] as implemented in the VASP code.[55] Core and valence electrons were treated with scalar relativistic corrections and configurations of Cs-$5s^25p^66s^1$, Pb-$5d^{10}6s^26p^2$, and I-$5s^25p^5$. Structural optimizations for unit cells of α- and δ-$CsPbI_3$ were performed with a cutoff energy of 600 eV and Γ-centered 8 × 8 × 8 and 8 × 4 × 2 Monkhorst−Pack special k-points until the magnitude of Hellmann−Feynman forces acting on atoms converged within 0.001 eV/Å. Using the determined lattice parameters of unit cells, (3 × 3 × 3) and (2 × 3 × 1) supercells were built for α- and δ-phases, respectively. Vacancy defects (V_{Cs}, V_{Pb}, and V_I), recognized to be the major point defects in halide perovskites,[40,42,43,56] were formed in the perfect supercells, and ionic relaxations with fixed lattice constants were followed with a cutoff energy of 400 eV and a force tolerance of 0.01 eV/Å using the Γ point only. When the optimized structures of defect-containing supercells were obtained, further total energy calculations were performed using denser 2 × 2 × 2 special k-points. For free molecules, one isolated molecule was put into the center of a supercell with a lattice constant of 15 Å and atomic relaxations were conducted to obtain the DFT total energy.

Finite size effects were considered in the monopole approximation with the calculated static dielectric constants of 19.5 and 12.4 for α- and δ-phases, respectively. The electrostatic potentials were aligned with respect to the semicore 5d peaks of Pb atoms at the same position (far away from the defect) in perfect and defective supercells. Band-filling effects were corrected for the shallow defects of V_I^0, V_{Cs}^0, V_{Pb}^0, and V_{Pb}^{-1}.

RESULTS AND DISCUSSION

Properties of Pristine $CsPbI_3$. We show the optimized lattice parameters of solids and bond lengths of molecules treated in this work in comparison with experiment in Table 1. The PBEsol functional reproduced the lattice parameters of crystals in good agreement with the experimental data, especially for α- and δ-$CsPbI_3$[17,42] (see Figure S1 for their optimized unit cells). The total energy per formula unit of α-phase was found to be 0.23 eV higher than that of δ-phase, indicating the aforementioned instability of cubic perovskite α-$CsPbI_3$ compared with the δ-phase.

The decomposition energies of $CsPbI_3$ to the constituents CsI and PbI_2 were determined to be −0.04 and 0.19 eV for α- and δ-phases, indicating that the α-phase spontaneously decomposes into the constituents, whereas the δ-phase decomposition is endothermic. The exothermic total energy difference (0.04 eV) between α-$CsPbI_3$ and PbI_2 + CsI—in agreement with other theoretical studies[42]—does not explain the stability of cubic $CsPbI_3$ at high temperature. As temperature increases, entropy can contribute to further deterioration of α-$CsPbI_3$ as shown in our former DFT result.[58] However, accepting recent insights into the nature of the α-phase as an average transitional state between the different lower symmetry phases through octahedral tilting,[19−22] the intrinsic thermal instability of cubic $CsPbI_3$ can be understood in terms of more stable polymorphs.

The calculated band gaps of α- and δ-$CsPbI_3$ are 1.19 and 2.45 eV, respectively. The calculated gap for the pristine cubic structure is smaller than the measured value of ca. 1.7 eV for the true α-phase but close to the predicted value (1.08 eV) by many-body perturbation theory, GW + SOC.[43]

Chemical Potentials of Solvated Ions. At standard conditions, the chemical potential variables of pure metals, solid compounds, and gases can be estimated using the DFT total energies. Following the procedure outlined above, the Gibbs free energies of formation of the solvated ions and the crystalline PbI_2 and CsI solids were determined to be $(\Delta G_f^{Cs^+})_{aq}^0(T_r) = -292.0$, $(\Delta G_f^{Pb^{2+}})_{aq}^0(T_r) = -24.4$, $(\Delta G_f^{I^-})_{aq}^0(T_r) = -51.6$, $(\Delta G_f^{PbI_2})_s^0(T_r) = -173.6$, and $(\Delta G_f^{CsI})_s^0(T_r) = -340.6$ kJ/mol.[49] From these values, the Gibbs free energies of dissociation of PbI_2 and CsI were

DOI: 10.1021/acs.jpcc.9b01552
J. Phys. Chem. C XXXX, XXX, XXX−XXX

calculated to be $(\Delta G_{dis}^{PbI_2})_s^0(T_r) = 46.0$ and $(\Delta G_{dis}^{CsI})_s^0(T_r) = -3.0$ kJ/mol using eqs 13 and 14. These values are consistent with the large difference in their solubility.[49,51]

To consider the constraints for the chemical potentials, the total energies of perfect and vacancy-containing (V_{Cs}^-, V_{Pb}^{-2}, and V_I^+) supercells for both phases were calculated, Figure 1. As the

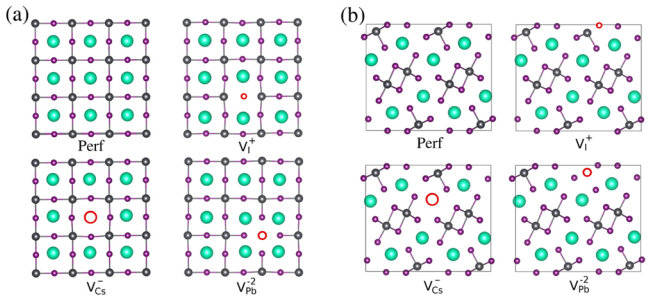

Figure 1. Optimized crystal structures of perfect and vacancy-containing supercells of (a) α- and (b) δ-$CsPbI_3$. Red circles indicate the spatial position of the site vacancies of V_{Cs}^-, V_{Pb}^{-2}, and V_I^+.

δ-phase is stable at room temperature, eq 17 is satisfied for chemical potentials of all kinds of ions. For the metastable α-phase, however, only the chemical potentials of Pb^{2+} and I^- ions satisfy the constraint of eq 17 because the Pb–I bonding characteristics in PbI_6 octahedra is similar in the two phases of $CsPbI_3$ (Figure S1). The Pb–I bond lengths in α- and δ-phases are 3.12 Å and 3.08–3.33 Å, which are similar to 3.21 Å in PbI_2 with a very low solubility,[49] implying high formation energies of Pb and I vacancies at their standard molalities. Moreover, we can assume that the Pb^{2+} ions placed in iodine octahedra are less prone to be lost than the I^- ions at the same molalities because of the stronger electrostatic interaction.[59] Otherwise, the second constraint eq 18 is applied to the chemical potentials of ions for both the phases. In order to find the solution ranges as narrow as possible, we made a systematic variation of the minimum value of chemical potential of I^- ions from 0.7 to 1.2 eV with an interval value of 0.1 eV, resulting in the several sets of solutions with the corresponding squared residual norms (errors) as shown in Figure 2. The solutions with a minimum error of 0.11 eV were determined to be $(\mu_I^-)_{aq}^0(T_r) = 0.93 \pm 0.07$, $(\mu_{Cs}^+)_{aq}^0(T_r) = -5.70 \mp 0.07$, $(\mu_{Pb}^{2+})_{aq}^0(T_r) = -8.67 \mp 0.14$, and $(\mu_H^+)_{aq}^0(T_r) = -5.74 \mp 0.07$ eV. These chemical potentials of ions at the reference state can be extended to those at any temperature and molality using eq 19.

Point Defect Processes. For vacancy point defects such as V_{Cs}, V_{Pb}, and V_I in α- and δ-$CsPbI_3$, we applied both the conventional (eq 1) and newly developed methods (eq 2) to calculate the formation energies. Thermodynamic equilibrium can be represented by either neutral or charged constituent species as follows:

$$\mu_{Cs} + \mu_{Pb} + 3\mu_I = \mu_{CsPbI_3} = \mu_{Cs}^+ + \mu_{Pb}^{2+} + \mu_I^- \quad (21)$$

$$\mu_{Pb} + 2\mu_I = \mu_{PbI_2} = \mu_{Pb}^{2+} + 2\mu_I^- \quad (22)$$

$$\mu_{Cs} + \mu_I = \mu_{CsI} = \mu_{Cs}^+ + \mu_I^- \quad (23)$$

Figure 3 shows the vacancy formation energies in α- and δ-phases based on the neutral species in a conventional way, where the environmental condition is described by the chemical potentials of neutral species satisfying the left-hand side of eqs 21–23. Here, neutral I-rich and Pb-rich conditions correspond to bulk phases (see Table 1), whereas the poor conditions can be determined from eq 22 with an assumption of $\mu_{PbI_2} \approx EDFT(PbI_2)$.[39] As bulk CsI is unlikely to coexist with $CsPbI_3$ because of its higher solubility than $CsPbI_3$ and PbI_2,[49] the assumption $\mu_{CsI} \approx E_{DFT}(CsPbI_3) - E_{DFT}(PbI_2)$ is considered in eq 23 to derive Cs-rich and Cs-poor conditions. In both I-poor (Pb- and Cs-rich) and I-rich (Pb- and Cs-poor) conditions, the δ-phase exhibits higher formation energies of vacancies (V_I, V_{Pb}, and V_{Cs}) than α-phase, indicating the higher stability of δ-phase. In the δ-phase, the thermodynamic transition level $\varepsilon(0/+1)$ of V_I is located about 0.44 eV below the conduction band minimum (CBM) and $\varepsilon(-1/-2)$ of V_{Pb} is found 0.52 eV above the VBM, indicating a deep-trap behavior resulting from the weaker Pb 6s–I 5p antibonding character when compared with α-phase.[42] A similar defect

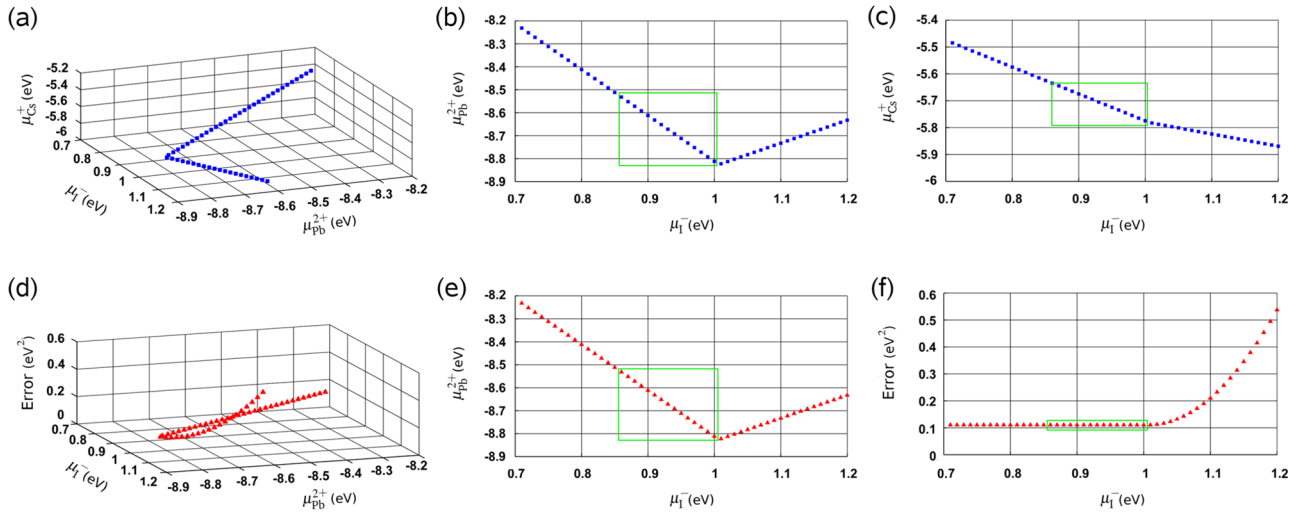

Figure 2. (a) Chemical potential ranges of ions (μ_{Cs}^+, μ_{Pb}^{2+}, and μ_I^-) optimized with different constraints for the minimum value of μ_I^- from 0.7 to 1.2 eV and their projections on (b) μ_I^-–μ_{Pb}^{2+} and (c) μ_I^-–μ_{Cs}^+ planes. (d) Corresponding square errors to the optimized chemical potentials and their projections on (e) μ_I^-–μ_{Pb}^{2+} and (f) μ_I^--error planes. Green rectangles include the solution points with a minimum error of 0.11 eV.

DOI: 10.1021/acs.jpcc.9b01552
J. Phys. Chem. C XXXX, XXX, XXX–XXX

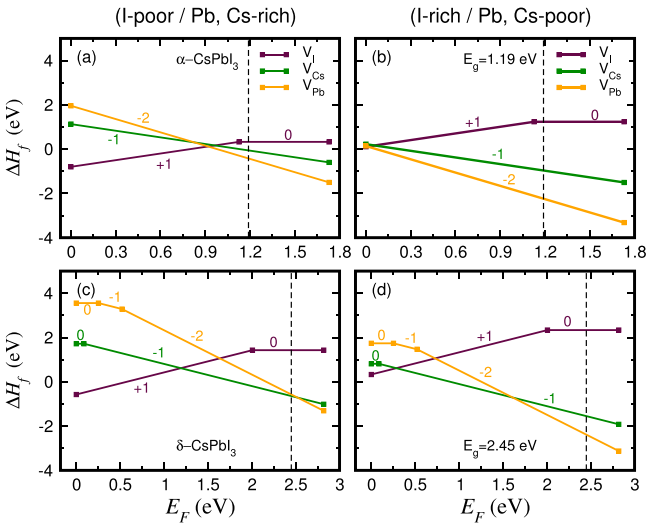

Figure 3. Formation energies of vacancy point defects as a function of Fermi energy E_F under I-poor (Cs- and Pb-rich) conditions (left panel) and I-rich (Cs- and Pb-poor) conditions (right panel) in (a,b) α-$CsPbI_3$ and (c,d) δ-$CsPbI_3$. The energies are calculated with respect to elemental standard states (conventional procedure). The dashed vertical lines represent the calculated band gap (conduction band edge).

analysis has been conducted for α-phase[43] and δ-phase[42] with band gaps of 1.44 and 2.54 eV, respectively, using PBE without spin−orbit coupling (SOC), where all kinds of point defects in $CsPbI_3$ were discussed to guide defect engineering. As in the former results for $MAPbI_3$,[39,40] this does not point out the exact experimental conditions, especially, for the solution-based fabrication.

On the basis of the determined chemical potentials of ions, which depend on physical parameters such as concentration and temperature of the solution, we can estimate the formation energies of vacancy defects in $CsPbI_3$, Figure 4. In general, rich and poor conditions of Pb^{2+} ions correspond to extreme concentrations of 1 and 10^{-20} mol/kg at room temperature,

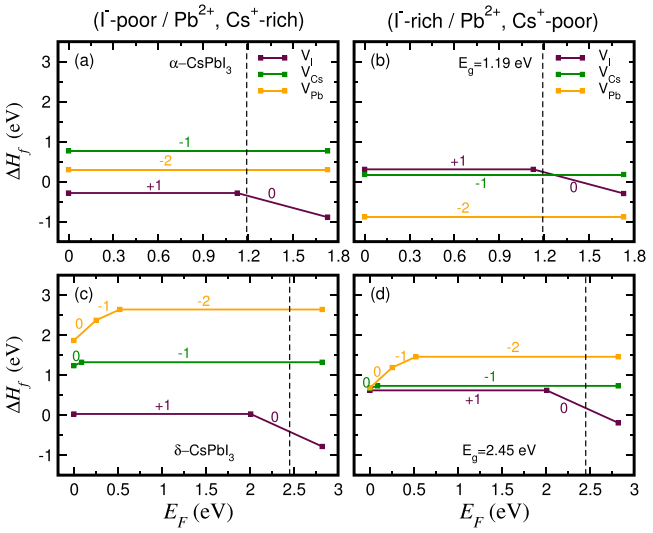

Figure 4. Formation energies of vacancy point defects with respect to ionic species (new procedure) as a function of E_F under I^--poor (Cs^+- and Pb^{2+}-rich) condition (left panel) and I^--rich (Cs^+- and Pb^{2+}-poor) condition (right panel) in (a,b) α-$CsPbI_3$ and (c,d) δ-$CsPbI_3$.

respectively. Using the right-hand side of eqs 21−23, the chemical potential limits of I^- and Cs^+ ions can be derived in a similar way to the neutral species. Any intermediate value of chemical potential between the lower and upper limits can be converted from concentration (or molality) of ions at certain temperatures using eq 19.

The slopes of formation energy against the Fermi energy E_F are different in the new approach (Figure 4) compared to the standard approach (Figure 3) for the same charge states. In particular, the formation energy lines of V_{Cs}, V_{Pb}, and V_I defects with charge states of −1, −2, and +1 are parallel (zero slopes) to the E_F axis for the cases of ionic species in both phases shown in Figure 4, indicating that the vacancy defects with their major charge states have formation energies independent of the Fermi energy, whereas for the cases of neutral species, they are observed to have some slopes as shown in Figure 3. The striking difference in vacancy formation energy originates from the distinct E_F coefficients: q in eq 1 for neutral species exchange versus $(q - \sum_i n_i q_i)$ in eq 2 for ionic species exchange. Importantly, the thermodynamic transition levels of the defects, $\varepsilon(q_1/q_2)$, remain unchanged.

Cubic Polymorph Stabilization through Vacancy Formation. We estimated the relative stabilization energies given by eq 20 in order to see whether α-$CsPbI_3$ can be stabilized over the δ-phase through vacancy formation. As can be seen in Figure 5, all the vacancy defects in neutral and

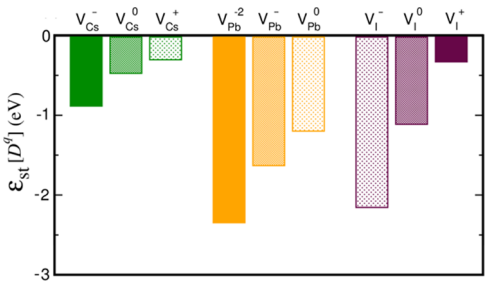

Figure 5. Relative stabilization energy per defect of α-phase over δ-phase $CsPbI_3$ through formation of vacancy defects with different charge states. Solid bars represent the major charge states of vacancies, while dotted bars show oxidized (for V_{Cs} and V_{Pb}) or reduced (for V_I) states.

charged states induce the stabilization of α-phase $CsPbI_3$, that is, there is a higher cost to forming a fixed concentration of defects in the δ-phase. Among three kinds of vacancy defects with major charge states, V_{Pb}^{-2} induces the biggest effect with the largest stabilization energy of −2.34 eV per defect, whereas V_I^+ improves the relative stability by only −0.31 eV. V_{Cs}^- has the middle value of −0.87 eV. Other vacancies with different charge states such as V_{Pb}^-, V_{Pb}^0, V_{Cs}^0, V_{Cs}^+, V_I^-, and V_I^0 also show stability improvement of α-phase with −1.62, −1.19, −0.46, −0.29, −2.15, and −1.10 eV, respectively. However, these defect charges are not stable in α-$CsPbI_3$, except V_I^0 that is stable in a shallow region below the CBM as shown in Figure 4a,b. These unstable charge states can be formed as intermediates between the stable states in δ- and α-phases so that the alternative transformation route, for example, V_{Pb}^0 (δ) → V_{Pb}^0 (α) → V_{Pb}^{-2} (α), can be supposed.

The total stabilization energy for a certain kind of vacancy defect can be obtained using the following equation:[38,40]

$$E_{st}[D^q](T) = \varepsilon_{st}[D^q]\cdot c(T) = \varepsilon_{st}[D^q]\cdot c_0\, e^{-H_f/k_BT} \quad (24)$$

DOI: 10.1021/acs.jpcc.9b01552
J. Phys. Chem. C XXXX, XXX, XXX−XXX

where $\varepsilon_{st}[D^q]$ is the stabilization energy per defect, c is the equilibrium concentration of defects, and H_f is the defect formation energy. From the requirement due to the internal energy difference of 0.23 eV/f.u. (21.8 kJ/mol or 9.29×10^{20} eV/cm^3) between the α- and δ-phases, the concentration of defects can be determined: 1.9% and $c = 3.9 \times 10^{20}$ cm^{-3} for V_{Pb}^{-2}, 5.6% and $c = 1.1 \times 10^{21}$ cm^{-3} for V_{Cs}^{-}, and 15.7% and $c = 3.0 \times 10^{21}$ cm^{-3} for V_I^{+}, which correspond to the remarkably low formation energies of 0.058, 0.033, or 0.006 eV at room temperature. As can be seen in Figure 4c,d, the formation energies of V_{Pb} and V_{Cs} in the δ-phase are much higher than these values even under their poor conditions, while V_I approaches this value under I$^-$-poor conditions. However, an abundance of iodine vacancies should be restrained because of its relatively low activation energy of migration (≈0.2−0.3 eV[28,56]), which may cause some serious problems for PSC performance.[39,60] It is important to find a way to create sufficient amount of cation vacancies, which are notably difficult to be formed at room temperature because of their higher formation energies in δ-phase.

Nanosizing Effect. Nanosizing offers a promising route. In fact, much increased surface-to-volume ratio of nanosized particles may promote the formation of vacancies on the surface, which will be followed by their diffusion into the bulk region. Accordingly, migration paths of cations from the inside bulk to the surface can also be shortened, resulting in the active formation of vacancies in the bulk. In actual experiment, it was found that the ratio of I/Pb is generally bigger than the stoichiometric ratio of 3:1 on the stable α-$CsPbI_3$ surface, ensuring the preferential formation of surface Pb vacancies.[56] Thus, former explanation for the nanosize effect as an increased contribution of surface energy to the internal energy compensation[9,11,17] is further amplified by a new microscopic mechanism related to the formation of cation vacancies.

Iodine-Rich Conditions. In concert with nanosizing, I$^-$-rich (Cs$^+$- and Pb^{2+}-poor) growth conditions can also facilitate the α-phase stability by lowering the formation energy of cation vacancies as mentioned above. In most experiments for achieving stable α-$CsPbI_3$ nanocrystals, this approach has been already followed. For instance, iodine sources such as excessive PbI_2 used in the anion exchange method[17,18,28] and anchoring molecules for 2D/3D perovskites[10,26,27] may realize I$^-$-rich conditions. The introduction of excess CsI has also been reported to improve the stability and efficiency of PSCs by composing the atom number ratio as Cs/Pb/I = 2:1:4, which provides the formation of Pb vacancies.[36] Advantageous effects of HI[10,16] and other metal iodides[61] on the α-phase stabilization can be interpreted similarly as originated from the decrease of Pb^{2+} and Cs$^+$ concentrations owing to the rise of I$^-$ concentration at the equilibrium state.

Ligand Engineering. The role of SCLs, also confirmed to further stabilize α-$CsPbI_3$, is likely based on a similar mechanism. As mentioned in the Introduction section, enhancement of stabilizing effect by replacing the conventional ligands such as OA with TOP,[30,31] TMPPA,[32] DPPA,[33] and IDA[15] can be attributed to the stronger interaction between the surface and the ligands, leading to the decrease of surface energy.[34] As reported by Wang et al.,[32] however, the ligands were not found to bind to the surface because the diffusion coefficient is much higher than that of bonded ligands, meaning that there is a rapid exchange of surface atom−ligand species such as Cs-oleate or Pb-oleate.[56] Paying careful attention to the suggested more effective ligands (TOP, TMPPA, DPPA, PVP, and IDA), it can be found that their functional groups tend to be more reductive or less Lewis acidic (than −COO$^-$ in OA) owing to their own functional properties or the chains they are linked in (see Figure S2). Ring structure chains such as aromatic or alicyclic compounds (DPPA and IDA) can support the reducibility of adjacent functional groups with the aid of conjugated electron clouds or nonpolarizable tendency, while multidentate (TOP and TMPPA) or polymeric (PVP) ligands may have a similar affection. More reductive functional groups are conducive to attract metallic cations such as Cs$^+$ and Pb^{2+} placed on a surface or in a solution to form bonding pairs. If the attraction is strong enough to fully extract metallic cations, bonding pairs will be desorbed from the surface to be free in a solution. Different charge transferences from OA and IDA to Pb atoms on the $CsPbI_3$ surface were shown by Pan et al.,[15] with which the superiority of IDA can be explained in respect of the above mechanism.

The schematic stabilization mechanism is shown in Figure 6. Because vacancies are considered as a source of the carrier

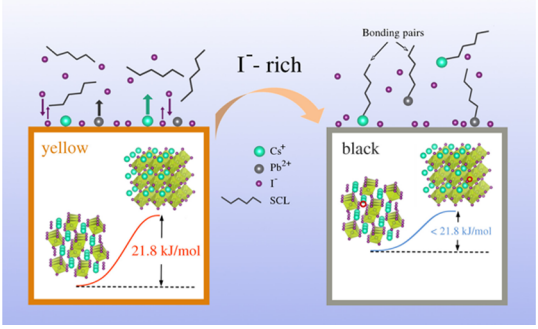

Figure 6. Schematic view of cubic-phase stabilization by introducing I$^-$-rich conditions and reductive SCLs. The I$^-$-rich condition allows extraction of metallic cations from the surface, which are covalently bonded to ligands in solution. Surface cation vacancies diffuse into the bulk region (marked with red circles) and reduce the internal energy difference between the black and yellow polymorphs.

recombination and chemical decomposition in PSCs,[4,40,41] the ligands that supply cations to passivate surface vacancies are mandatory to attain the phase stability and efficiency. Consequently, we postulate that partial or full extraction of metallic cations (especially Cs$^+$), leading to weakening of the chemical bonding between Cs and PbI_6 octahedra, is the driving force for the α-$CsPbI_3$ stability.

Extrinsic Doping. Finally, p-type (hole) doping offers an alternative route for phase stabilization. As shown in Figure 4d, V_{Pb}^{-2} has high formation energy and transforms to different charge states such as V_{Pb}^{-} and V_{Pb}^{0} with lower formation energies as E_F moves toward the VBM. The alternative transformation route of V_{Pb}^{0} (δ) → V_{Pb}^{0} (α) → V_{Pb}^{-2} (α) endows a larger energy improvement per defect than the one of V_{Pb}^{-2} (δ) → V_{Pb}^{-2} (α). Hence, making bulk $CsPbI_3$ p-type with E_F < 0.52 eV may be beneficial to the α-phase stabilization. It can be said that a divalent or trivalent cation doping effect[23,35,36] may be related to this route, although further theoretical and experimental investigations are needed to test this hypothesis.

CONCLUSIONS

In summary, we have investigated routes to stabilize the black α-phase of $CsPbI_3$ from an atomistic chemical perspective. A

DOI: 10.1021/acs.jpcc.9b01552
J. Phys. Chem. C XXXX, XXX, XXX−XXX

new ab initio thermodynamic formalism for defect formation in crystalline solids surrounded by solution, using the chemical potentials of the solvated ions, has been developed so that a realistic synthetic environment can be considered. This approach has wider implications for solution-processed materials.

For $CsPbI_3$, the formation energies of vacancy defects such as V_{Pb}, V_{Cs}, and V_I with different charge states were estimated by both the conventional defect method using the chemical potentials of neutral species and the new method using those of ionic species. It has been revealed that the α-$CsPbI_3$ stabilization is supported by formation of cation vacancies. The internal energy difference between the α- and δ-phases, representing the relative stability or energy barrier for stabilization, decreases upon creation of vacancy defects. It was shown that the established nanosizing effect originates not only from the surface energy gain compensating the stability difference but also from the weakening of bonding between Cs and PbI_6 octahedra through vacancy formation (cation extraction).

Growth conditions that are Cs^+- and/or Pb^{2+}-poor are beneficial to α-phase stabilization, which can be induced by I^--rich conditions or the use of SCLs that are prone to bind with metallic cations. I^--rich conditions can be realized by excess PbI_2 and CsI, or through the addition of other metal halides and HI, or even by halide-containing ligands. In stabilizing the α-phase, such ligands play an important role, and thus one should make efforts to select an efficient ligand containing more reductive functional groups. Other ligands that supply cationic groups to passivate the surface vacancies are also mandatory to reduce trap centers and achieve high PV performance along with the phase stability. Finally, we suggested to make a bulk material p-type doped with E_F close to the valence band as a promising way for the cubic polymorph stabilization.

We expect that these avenues are applicable to other perovskite compositions and can provide general guidelines for controlling phase stability beyond the standard temperature–pressure phase diagrams established for pristine bulk samples.

■ ASSOCIATED CONTENT

Supporting Information

The Supporting Information is available free of charge on the ACS Publications website at DOI: 10.1021/acs.jpcc.9b01552.

Optimized unit cell structures of α- and δ-$CsPbI_3$, constraints for the standard ionic chemical potentials according to eq 17, and molecular structures of TOP, TMPPA, DPPA, PVP, and IDA (PDF)

■ AUTHOR INFORMATION

Corresponding Authors

*E-mail: cj.yu@ryongnamsan.edu.kp (C.-J.Y.).
*E-mail: a.walsh@imperial.ac.uk (A.W.).

ORCID

Chol-Jun Yu: 0000-0001-9523-4325
Un-Gi Jong: 0000-0003-4654-2449
Shuzhou Li: 0000-0002-2159-2602
Aron Walsh: 0000-0001-5460-7033

Notes

The authors declare no competing financial interest.

■ ACKNOWLEDGMENTS

This work is supported as part of the fundamental research project "Design of Innovative Functional Materials for Energy and Environmental Application" (no. 2016-20) funded by the State Committee of Science and Technology, DPR Korea. The work in the UK has been supported by the Royal Society and the Leverhulme Trust.

■ REFERENCES

(1) Saliba, M. Perovskite solar cells must come of age. *Science* **2018**, *359*, 388–389.
(2) Saliba, M.; et al. Cesium-containing triple cation perovskite solar cells: improved stability, reproducibility and high efficiency. *Energy Environ. Sci.* **2016**, *9*, 1989–1997.
(3) Rehman, W.; McMeekin, D. P.; Patel, J. B.; Milot, R. L.; Milot, M. B. J.; Johnston, M. B.; Snaith, H. J.; Herz, L. M. Photovoltaic mixed-cation lead mixed-halide perovskites: links between crystallinity, photo-stability and electronic properties. *Energy Environ. Sci.* **2017**, *10*, 361–369.
(4) Saidaminov, M. I.; et al. Suppression of atomic vacancies via incorporation of isovalent small ions to increase the stability of halide perovskite solar cells in ambient air. *Nat. Energy* **2018**, *3*, 648–654.
(5) Syzgantseva, O. A.; Saliba, M.; Grätzel, M.; Rothlisberger, U. Stabilization of the Perovskite Phase of Formamidinium Lead Triiodide by Methylammonium, Cs, and/or Rb Doping. *J. Phys. Chem. Lett.* **2017**, *8*, 1191–1196.
(6) Yi, C.; Luo, J.; Meloni, S.; Boziki, A.; Ashari-Astani, N.; Grätzel, C.; Zakeeruddin, S. M.; Röthlisberger, U.; Grätzel, M. Entropic stabilization of mixed A-cation ABX_3 metal halide perovskites for high performance perovskite solar cells. *Energy Environ. Sci.* **2016**, *9*, 656–662.
(7) Lee, J.-W.; Kim, D.-H.; Kim, H.-S.; Seo, S.-W.; Cho, S. M.; Park, N.-G. Formamidinium and Cesium Hybridization for Photo- and Moisture-Stable Perovskite Solar Cell. *Adv. Energy Mater.* **2015**, *5*, 1501310.
(8) Duong, T.; et al. Rubidium Multication Perovskite with Optimized Bandgap for Perovskite-Silicon Tandem with over 26% Efficiency. *Adv. Energy Mater.* **2017**, *7*, 1700228.
(9) Ahmad, W.; Khan, J.; Niu, G.; Tang, J. Inorganic $CsPbI_3$ Perovskite-Based Solar Cells: A Choice for a Tandem Device. *Sol. RRL* **2017**, *1*, 1700048.
(10) Zhang, T.; Dar, M. I.; Li, G.; Xu, F.; Guo, N.; Grätzel, M.; Zhao, Y. Bication lead iodide 2D perovskite component to stabilize inorganic α-$CsPbI_3$ perovskite phase for high-efficiency solar cells. *Sci. Adv.* **2017**, *3*, No. e1700841.
(11) Swarnkar, A.; Marshall, A. R.; Sanehira, E. M.; Chernomordik, B. D.; Moore, D. T.; Christians, J. A.; Chakrabarti, T.; Luther, J. M. Quantum dot-induced phase stabilization of α-$CsPbI_3$ perovskite for high-efficiency photovoltaics. *Science* **2016**, *354*, 92.
(12) Li, X.; Yu, D.; Cao, F.; Gu, Y.; Wei, Y.; Wu, Y.; Song, J.; Zeng, H. Healing All-Inorganic Perovskite Films via Recyclable Dissolution-Recyrstallization for Compact and Smooth Carrier Channels of Optoelectronic Devices with High Stability. *Adv. Funct. Mater.* **2016**, *26*, 5903.
(13) Ramasamy, P.; Lim, D.-H.; Kim, B.; Lee, S.-H.; Lee, M.-S.; Lee, J.-S. All-inorganic cesium lead halide perovskite nanocrystals for photodetector applications. *Chem. Commun.* **2016**, *52*, 2067.
(14) Cho, H.; et al. Overcoming the electroluminescence efficiency limitations of perovskite light-emitting diodes. *Science* **2015**, *350*, 1222.
(15) Pan, J.; et al. Bidentate Ligand-Passivated $CsPbI_3$ Perovskite Nanocrystals for Stable Near-Unity Photoluminescence Quantum Yield and Efficient Red Light-Emitting Diodes. *J. Am. Chem. Soc.* **2018**, *140*, 562–565.
(16) Eperon, G. E.; Paternò, G. M.; Sutton, R. J.; Zampetti, A.; Haghighirad, A. A.; Cacialli, F.; Snaith, H. J. Inorganic caesium lead iodide perovskite solar cells. *J. Mater. Chem. A* **2015**, *3*, 19688–19695.

DOI: 10.1021/acs.jpcc.9b01552
J. Phys. Chem. C XXXX, XXX, XXX–XXX

(17) Protesescu, L.; Yakunin, S.; Bodnarchuk, M. I.; Krieg, F.; Caputo, R.; Hendon, C. H.; Yang, R. X.; Walsh, A.; Kovalenko, M. V. Nanocrystals of Cesium Lead Halide Perovskites ($CsPbX_3$, X = Cl, Br, and I): Novel Optoelectronic Materials Showing Bright Emission with Wide Color Gamut. *Nano Lett.* **2015**, *15*, 3692−3696.
(18) Hoffman, J. B.; Schleper, A. L.; Kamat, P. V. Transformation of Sintered $CsPbBr_3$ Nanocrystals to Cubic $CsPbI_3$ and Gradient $CsPbBrxI_{3-x}$ through Halide Exchange. *J. Am. Chem. Soc.* **2016**, *138*, 8603−8611.
(19) Bertolotti, F.; Protesescu, L.; Kovalenko, M. V.; Yakunin, S.; Cervellino, A.; Billinge, S. J. L.; Terban, M. W.; Pedersen, J. S.; Masciocchi, N.; Guagliardi, A. Coherent Nanotwins and Dynamic Disorder in Cesium Lead Halide Perovskite Nanocrystals. *ACS Nano* **2017**, *11*, 3819−3831.
(20) Yang, R. X.; Skelton, J. M.; da Silva, E. L.; Frost, J. M.; Walsh, A. Spontaneous Octahedral Tilting in the Cubic Inorganic Cesium Halide Perovskites $CsSnX_3$ and $CsPbX_3$ (X = F, Cl, Br, I). *J. Phys. Chem. Lett.* **2017**, *8*, 4720−4726.
(21) Marronnier, A.; Roma, G.; Boyer-Richard, S.; Pedesseau, L.; Jancu, J.-M.; Bonnassieux, Y.; Katan, C.; Stoumpos, C. C.; Kanatzidis, M. G.; Even, J. Anharmonicity and Disorder in the Black Phases of Cesium Lead Iodide Used for Stable Inorganic Perovskite Solar Cells. *ACS Nano* **2018**, *12*, 3477−3486.
(22) Marronnier, A.; Lee, H.; Geffroy, B.; Even, J.; Bonnassieux, Y.; Roma, G. Structural Instabilities Related to Highly Anharmonic Phonons in Halide Perovskites. *J. Phys. Chem. Lett.* **2017**, *8*, 2659−2665.
(23) Lau, C. F. J.; et al. Enhanced performance via partial lead replacement with calcium for a $CsPbI_3$ perovskite solar cell exceeding 13% power conversion efficiency. *J. Mater. Chem. A* **2018**, *6*, 5580−5586.
(24) Sutton, R. J.; et al. Bandgap-Tunable Cesium Lead Halide Perovskites with High Thermal Stability for Efficient Solar Cells. *Adv. Energy Mater.* **2016**, *6*, 1502458.
(25) Dastidar, S.; Egger, D. A.; Tan, L. Z.; Cromer, S. B.; Dillon, A. D.; Liu, S.; Kronik, L.; Rappe, A. M.; Fafarman, A. T. High Chloride Doping Levels Stabilize the Perovskite Phase of Cesium Lead Iodide. *Nano Lett.* **2016**, *16*, 3563.
(26) Li, F.; Pei, Y.; Xiao, F.; Zeng, T.; Yang, Z.; Xu, J.; Sun, J.; Peng, B.; Liu, M. Tailored dimensionality to regulate the phase stability of inorganic cesium lead iodide perovskites. *Nanoscale* **2018**, *10*, 6318−6322.
(27) Liao, J.-F.; Rao, H.-S.; Chen, B.-X.; Kuang, D.-B.; Su, C.-Y. Dimension engineering on cesium lead iodide for efficient and stable perovskite solar cells. *J. Mater. Chem. A* **2017**, *5*, 2066−2072.
(28) Nedelcu, G.; Protesescu, L.; Yakunin, S.; Bodnarchuk, M. I.; Grotevent, M. J.; Kovalenko, M. V. Fast Anion-Exchange in Highly Luminescent Nanocrystals of Cesium Lead Halide Perovskites ($CsPbX_3$, X = Cl, Br, I). *Nano Lett.* **2015**, *15*, 5635−5640.
(29) Akkerman, Q. A.; D'Innocenzo, V.; Accornero, S.; Scarpellini, A.; Petrozza, A.; Prato, M.; Manna, L. Tuning the Optical Properties of Cesium Lead Halide Perovskite Nanocrystals by Anion Exchange Reactions. *J. Am. Chem. Soc.* **2015**, *137*, 10276−10281.
(30) Liu, F.; et al. Highly luminescent phase-stable $CsPbI_3$ perovskite quantum dots achieving near 100% absolute photoluminescence quantum yield. *ACS Nano* **2017**, *11*, 10373−10383.
(31) Lu, C.; Li, H.; Kolodziejski, K.; Dun, C.; Huang, W.; Carroll, D.; Geyer, S. M. Enhanced stabilization of inorganic cesium lead triiodide ($CsPbI_3$) perovskite quantum dots with tri-octylphosphine. *Nano Res.* **2018**, *11*, 762−768.
(32) Wang, C.; Chesman, A. S. R.; Jasieniak, J. J. Stabilizing the cubic perovskite phase of $CsPbI_3$ nanocrystals by using an alkyl phosphinic acid. *Chem. Commun.* **2017**, *53*, 232−235.
(33) Mubiayi, K. P.; Moloto, N.; Moloto, M. J. Effect of diphenyl phosphinic acid on cesium lead iodide perovskite stability. *CrystEngComm* **2018**, *20*, 5275−5280.
(34) Li, B.; Zhang, Y.; Fu, L.; Yu, T.; Zhou, S.; Zhang, L.; Yin, L. Surface passivation engineering strategy to fully-inorganic cubic $CsPbI_3$ perovskites for high-performance solar cells. *Nat. Commun.* **2018**, *9*, 1076.
(35) Hu, Y.; Bai, F.; Liu, X.; Ji, Q.; Miao, X.; Qiu, T.; Zhang, S. Bismuth incorporation stabilized α-$CsPbI_3$ for fully inorganic perovskite solar cells. *ACS Energy Lett.* **2017**, *2*, 2219−2227.
(36) Xiang, S.; Li, W.; Wei, Y.; Liu, J.; Liu, H.; Zhu, L.; Chen, H. The synergistic effect of non-stoichiometry and Sb-doping on air-stable α-$CsPbI_3$ for efficient carbon-based perovskite solar cells. *Nanoscale* **2018**, *10*, 9996−10004.
(37) Butler, K. T.; Walsh, A.; Cheetham, A. K.; Kieslich, G. Organised chaos: entropy in hybrid inorganic-organic systems and other materials. *Chem. Sci.* **2016**, *7*, 6316−6324.
(38) Freysoldt, C.; Grabowski, B.; Hickel, T.; Neugebauer, J.; Kresse, G.; Janotti, A.; de Walle, C. G. V. First-principles calculations for point defects in solids. *Rev. Mod. Phys.* **2014**, *86*, 253−305.
(39) Kye, Y.-H.; Yu, C.-J.; Jong, U.-G.; Chen, Y.; Walsh, A. Critical Role of Water in Defect Aggregation and Chemical Degradation of Perovskite Solar Cells. *J. Phys. Chem. Lett.* **2018**, *9*, 2196−2201.
(40) Buin, A.; Pietsch, P.; Xu, J.; Voznyy, O.; Ip, A. H.; Comin, R.; Sargent, E. H. Materials Processing Routes to Trap-Free Halide Perovskites. *Nano Lett.* **2014**, *14*, 6281−6286.
(41) Agiorgousis, M. L.; Sun, Y.-Y.; Zeng, H.; Zhang, S. Strong Covalency-Induced Recombination Centers in Perovskite Solar Cell Material $CH_3NH_3PbI_3$. *J. Am. Chem. Soc.* **2014**, *136*, 14570−14575.
(42) Huang, Y.; Yin, W.-J.; He, Y. Intrinsic Point Defects in Inorganic Cesium Lead Iodide Perovskite $CsPbI_3$. *J. Phys. Chem. C* **2018**, *122*, 1345.
(43) Li, Y.; Zhang, C.; Zhang, X.; Huang, D.; Shen, Q.; Cheng, Y.; Huang, W. Intrinsic Point Defects in Inorganic perovskite $CsPbI_3$ from first-principles prediction. *Appl. Phys. Lett.* **2017**, *111*, 162106.
(44) Walsh, A. Principles of Chemical Bonding and Band Gap Engineering in Hybrid Organic—Inorganic Halide Perovskites. *J. Phys. Chem. C* **2015**, *119*, 5755−5860.
(45) Clark, S. J.; Robertson, J.; Lany, S.; Zunger, A. Intrinsic defects in ZnO calculated by screened exchange and hybrid density functionals. *Phys. Rev. B: Condens. Matter Mater. Phys.* **2010**, *81*, 115311.
(46) Kumagai, Y.; Burton, L. A.; Walsh, A.; Oba, F. Electronic Structure and Defect Physics of Tin Sulfides: SnS, Sn_2S_3, and SnS_2. *Phys. Rev. Appl.* **2016**, *6*, 014009.
(47) Yan, Q.; Janotti, A.; Scheffler, M.; Van de Walle, C. G. Role of nitrogen vacancies in the luminescence of Mg-doped GaN. *Appl. Phys. Lett.* **2012**, *200*, 142110.
(48) O'Brien, C. J.; Rák, Z.; Brenner, D. Free energies of (Co, Fe, Ni, Zn)Fe2O4 spinels and oxides in water at high temperatures and pressure from density functional theory: results for stoichiometric NiO and NiFe2O4 surfaces. *J. Phys.: Condens. Matter* **2013**, *25*, 445008.
(49) *CRC Handbook of Chemistry and Physics*, internet version 2005; Lide, D. R., Ed.; CRC Press: Boca Raton, FL; 2005, http://www.hbcpnetbase.com.
(50) Reuter, K.; Scheffler, M. First-Principles Atomistic Thermodynamics for Oxidation Catalysis: Surface Phase Diagrams and Catalytically Interesting Regions. *Phys. Rev. Lett.* **2003**, *90*, 046103.
(51) Tenuta, E.; Zheng, C.; Rubel, O. Thermodynamic origin of instability in hybrid halide perovskites. *Sci. Rep.* **2016**, *6*, 37654.
(52) *Handbook of oOrganic Solvent Properties*; Smallwood, I. M., Ed.; Arnold, 1996.
(53) Kresse, G.; Joubert, D. From ultrasoft pseudopotentials to the projector augmented-wave method. *Phys. Rev. B: Condens. Matter Mater. Phys.* **1999**, *59*, 1758.
(54) Perdew, J. P.; Ruzsinszky, A.; Csonka, G. I.; Vydrov, O. A.; Scuseria, G. E.; Constantin, L. A.; Zhou, X.; Burke, K. Restoring the Density Gradient Expansion for Exchange in Solids and Surfaces. *Phys. Rev. Lett.* **2008**, *100*, 136406.
(55) Kresse, G.; Furthmüller, J. Efficiency of ab-initio total energy calculations for metals and semiconductors using a plane-wave basis set. *Comput. Mater. Sci.* **1996**, *6*, 15−50.

DOI: 10.1021/acs.jpcc.9b01552
J. Phys. Chem. C XXXX, XXX, XXX−XXX

(56) Li, X.; et al. All inorganic halide perovskites nanosystem: Synthesis, structural features, optical properties and optoelectonic applications. *Small* **2017**, *13*, 1603996.
(57) Stoumpos, C. C.; Malliakas, C. D.; Kanatzidis, M. G. Semiconducting tin and lead iodide perovskites with organic cations: phase transitions, high mobilities, and near-infrared photoluminescent properties. *Inorg. Chem.* **2013**, *52*, 9019−9038.
(58) Jong, U.-G.; Yu, C.-J.; Kye, Y.-H.; Kim, Y.-S.; Kim, C.-H.; Ri, S.-K. A first-principles study on the chemical stability of inorganic perovskite solid solutions $Cs_{1-x}Rb_xPbI_3$ at finite temperature and pressure. *J. Mater. Chem. A* **2018**, *6*, 17994−18002.
(59) Walsh, A.; Scanlon, D. O.; Chen, S.; Gong, X. G.; Wei, S.-H. Self-regulation mechanism for charged point defects in hybrid halide perovskites. *Angew. Chem., Int. Ed.* **2015**, *54*, 1791−1794.
(60) Eames, C.; Frost, J. M.; Barnes, P. R.; O'Regan, B. C.; Walsh, A.; Islam, M. S. Ionic transport in hybrid lead iodide perovskite solar cells. *Nat. Commun.* **2015**, *6*, 7497.
(61) Woo, J. Y.; Kim, Y.; Bae, J.; Kim, T. G.; Kim, J. W.; Lee, D. C.; Jeong, S. Highly Stable Cesium Lead Halide Perovskite Nanocrystals through in Situ Lead Halide Inorganic Passivation. *Chem. Mater.* **2017**, *29*, 7088−7092.

DOI: 10.1021/acs.jpcc.9b01552
J. Phys. Chem. C XXXX, XXX, XXX−XXX